Exploration of changes in the chemical composition of sedimentary organic matter and the underlying processes during biodegradation through advanced analytical techniques

Morgane Derrien, Laurent Jeanneau, Emilie Jardé, Jin Hur, Sunghwan Kim

Exploration of changes in the chemical composition of sedimentary organic matter and the underlying processes during biodegradation through advanced analytical techniques

Morgane Derrien[1,2,*], Laurent Jeanneau[3], Emilie Jardé[3], Jin Hur[1], and Sunghwan Kim[4,5]

[1]*Department of Environment and Energy, Sejong University, Seoul 05006, South Korea*

[2]*Instituto de Ciencias Agroalimentarias, Animales y Ambientales, Universidad de O'Higgins, San Fernando, Chile*

[3]*Centre National de la Recherche Scientifique (CNRS), Géosciences Rennes – UMR 6118, Université de Rennes 1, 35042 Rennes, France*

[4]*Department of Chemistry, Kyungpook National University, Daegu 41566, South Korea*

[5]*Mass Spectrometry Based Convergence Research Center, Daegu 41566, South Korea*

* Corresponding author

E-Mail: morgane.derrien@uoh.cl

Abstract

Rationale. Although the scientific community widely investigated the organic matter biodegradation processes, only a limited number of studies have explored the molecular changes of this material while its structure, composition, and origin play a key in these processes. **Methodology.** In this context, we decided to examine the effects of the biodegradation on the chemical composition of sedimentary organic matter and to explore the underlying mechanisms. We conceived a laboratory-based degradation experiment utilizing organic-rich sediments artificially composed of two contrasting organic matter end-members (i.e., soil and algae) under two oxygen conditions. The sediment samples before and after incubation were then analyzed via laser desorption/ionization Fourier transform ion cyclotron resonance mass spectrometry for molecular characterization and via thermally assisted hydrolysis and methylation gas chromatography–mass spectrometry in order to offer insights into the mechanisms driving biodegradation processes. **Results.** Our results from molecular characterization unveiled distinct pathways of biodegradation contingent upon the source material. Moreover, they hinted at a predilection for altering high molecular weight compounds like lignin/CRAM and CAS compounds, manifesting as a conversion into lower molecular weight counterparts. Furthermore, the complementary findings from biomarker analyses underscored the influence of environmental factors - specifically oxygen conditions and microbial communities - on organic matter decomposition. **Discussion.** Although this study is a controlled laboratory experiment and more studies are needed, it demonstrated the intricate interplay among chemical, biological, and environmental factors, profoundly shaping the reactivity of organic matter. This study underscores the critical need for persistent inquiry, aimed at unraveling the factors and conditions governing the diverse pathways of biodegradation.

Keywords: Sedimentary organic matter; Biodegradation; Molecular characterization; LDI FT–ICR MS; Biomarkers.

1. Introduction

Sediments operate as sources and sinks of nutrients and pollutants in aquatic systems. They also represent a large reservoir of organic matter (OM) from diverse sources (e.g., terrestrial, aquatic, estuarine, marine, etc.) and in various proportions according to the environment, region, and hydrology. Indeed, sedimentary OM is derived from aquatic material such as algae, bacteria, plankton, macrophytes, and nekton formed in situ, but also receives terrestrial OM such as soil, vascular plants, leaves, root exudates and anthropogenic OM ~~such as soil OM~~, which is easily transported from the upstream catchment into rivers through hydrological processes, finally ending up in sediments (Briand et al. 2015; Jeanneau et al. 2018; van der Meij et al. 2018). Sediments are also a reactive compartment where diagenetic processes occur, inducing physical, chemical, and/or biological changes to the sedimentary OM (Henrichs 1992; Kuznetsova et al. 2019; Milliken 2003). Among the diagenetic processes, biodegradation plays a key role in OM biogeochemistry as it is one of the main processes causing changes in its amount, composition, and properties in aquatic systems (Moran et al., 2000; Arndt et al., 2013; Sankar et al., 2019; Derrien et al., 2019a).

OM biodegradation is based on the common preconception that OM is represented as a mix of recalcitrant materials usually associated with terrestrial origin and labile materials associated with aquatic OM (Hansell 2013). OM biodegradation is often oversimplified and/or restricted to preferential degradation of labile and/or low molecular weight (LMW) organic compounds leading to the rapid loss of them rather than the recalcitrant material like lignin and high molecular weight (HMW) organic compounds (Curtis-Jackson et al. 2009; Hach et al. 2020; Hansen et al. 2016; Moran and Zepp 1997; Ward et al. 2019). However, since the early

2000s, new paradigms on the stability of terrestrial OM and more specifically on soil OM have been proposed (Wershaw 2004). They conceptualized soil OM stabilization as the result of a combination of physical factors controlling its accessibility (Lützow et al. 2006) as well as chemical factors such as its oxidizing degree controlling the energy available for microorganisms (LaRowe and Van Cappellen 2011). Even recalcitrance as an intrinsic property of molecules has been questioned arguing that under favorable environmental conditions, all organic molecules would be biodegradable (Kleber 2010). These paradigms are in line with what was observed in several studies where a preferential conversion of high molecular weight (HMW) compounds into reactive and bioavailable LMW compounds were observed (Kellerman et al. 2015; Kothawala et al. 2020; Liu et al. 2019). In the literature, biodegradation processes have also been associated with the production of HMW aromatic material through alteration and recombination of existing compounds (e.g., large organic biomolecules or humification processes) (Hach et al. 2020; Kleber and Lehmann 2019; Lee et al. 2016). These various scenarios of biodegradation processes and our difficulties in finding a consensus on the biodegradation mechanisms and pathways are related not only to the characteristics of OM itself such as composition and sources but also to the characteristics and properties of the ecosystem (i.e., physiochemical conditions and biological communities) (D'Andrilli et al. 2019; Kothawala et al. 2020; McCallister et al. 2018). Furthermore, priming effects represent a potentially important mechanism underlying the biodegradation of OM in aquatic systems complexifying our understanding (Bianchi 2011; Bianchi and Ward 2019; Zhuang et al. 2021). Priming effects refer to quantitative and qualitative changes in the microbial decomposition of recalcitrant OM upon the addition of labile OM (Guenet et al. 2014, 2010a). They are delineated as negative, neutral, or positive effects depending on the consequences in the ways that they may reduce or exert no effect on or stimulate OM biodegradation (B Guenet et al., 2010; Gontikaki et al., 2013; Ward et al., 2016, 2019; Bengtsson et al., 2018; Derrien et al.,

2019c). All these discrepancies in the observed biodegradation mechanisms coupled with the no consensus on the occurrence and role of priming effects result in a critical need for more studies focused on the biodegradation processes and mechanisms through approaches combining analyses providing quantitative and qualitative information (D'Andrilli et al. 2019). Most of the biodegradation studies in the literature aim at quantifying the OM degradation and mineralization, and its kinetic through microbial biomass measurement, dissolved organic carbon or CO_2 concentrations/fluxes (Bowen et al. 2009; Kalbitz et al. 2003; Moran et al. 2000; Sankar et al. 2019; Vähätalo et al. 2010). Only a few studies target the qualitative aspect of the biodegradation processes (i.e., exploration of the molecular changes) while the structure and composition of OM play a key in these processes (Arndt et al. 2013; Herzsprung et al. 2017; Kellerman et al. 2015; Kothawala et al. 2020). Yet, investigating these molecular changes in similar conditions will not only allow us to lighten our knowledge of biodegradation concepts but also provide a chemical fingerprint that helps the understanding of OM reactivity and metabolism. Additionally, the few studies exploring the molecular composition during biodegradation are limited to the dissolved fraction while two fractions exist (i.e., particulate and dissolved) and both are intimately linked to each other (Derrien et al. 2019a). Hence, we decided to tackle this knowledge gap by investigating the compositional changes of sedimentary OM during biodegradation in this study.

Due to the high heterogeneity and complexity of the OM composition related to its dynamics, involvement in a large number of biogeochemical processes, and the type of environment, we have decided to head toward a laboratory experiment for this study. Indeed, controlled laboratory experiments offer the benefits of providing in-depth insight into the effects of selected parameters have on OM composition, in contrast with field samples that only represent a snapshot in space and time. The controlled laboratory degradation experiment was conducted using organic-rich sediments artificially composed of two contrasting OM end-

124 members (i.e., soil and algae) at known mixing ratios and under two oxygen conditions (oxic
125 and anoxic). The molecular changes induced by biodegradation in sediments and the
126 mechanisms behind them were investigated through two advanced analytical tools: laser
127 desorption/ionization Fourier transform ion cyclotron resonance mass spectrometry (LDI FT–
128 ICR MS) and thermally assisted hydrolysis and methylation gas chromatography-mass
129 spectrometry (THM–GC–MS). Currently, high-resolution mass spectrometry techniques such
130 as FT–ICR MS are likely considered as the most powerful tool used to characterize the OM
131 molecular properties (Kellerman et al. 2015; Valle et al. 2018). The LDI FT–ICR MS technique
132 was chosen as it represents a direct and highly sensitive analysis at the molecular level to
133 explore the biodegradation-induced changes in chemical composition in sedimentary OM. The
134 second technique was selected to explore the biomarker fingerprints to obtain clues to
135 understand the underlying processes during biodegradation (Meyers and Ishiwatari 1993;
136 Wakeham and Ertel 1988). Both techniques were also selected as they present the advantage
137 of being able to directly analyze artificial sediments without any pre-treatment step such as
138 chemical extraction and thus limiting modifications of the sample (Aubriet and Carré 2019).
139 The main goal of this study was to provide a detailed exploration of the molecular composition
140 changes of sedimentary OM induced by biodegradation and evaluate the role of factors such as
141 type of sources and oxygen on it. The study specifically aimed at answering the following
142 questions: (i) what molecules or groups of molecules are the most affected by biodegradation
143 processes, (ii) what is the potential effect of OM source or oxygen conditions (i.e., oxic versus
144 anoxic) on biodegradation processes? and (iii) what are the underlying processes behind
145 biodegradation?
146
147 **2. Material and methods**
148 *2.1. Experimental design of the incubation experiment*

Two contrasted end-members (i.e., soil and algae) were mixed at soil-to-algae ratios (S:A) of 100:0, 75:25, 50:50, 25:75, and 0:100, based on the organic carbon (OC) concentrations (Derrien et al. 2019b). In natural aquatic systems, ratios between both OM sources greatly vary according to the season and the hydrology. Therefore, we decided to perform the study at several ratios. The soil end-member (topsoil, 0-10cm) was collected at Bukhansan National Park, South Korea (37°43'37.0" N 127°00'50.9"), a fully forested area composed of broadleaved trees such as *Quercus mongolica*, *Q. serrata*, the coniferous tree, *Pinus densiflora*, and the *Robinia pseudoacacia* plantation (Choi and Yang 2012). A commercial unicellular green alga (*Chlorella vulgaris*), which is commonly found in freshwaters and marine environments, was purchased from Aquanet Co., Ltd. in Gyeongsangnam-do, South Korea, and used as the algae end-member. Further details regarding the end-members and the experiment can be found in Derrien et al. 2019c. Briefly, incubation experiments in oxic and anoxic conditions were performed in pre-washed and pre-combusted (450 °C for 4 hours) 125 ml Wheaton® amber glass bottles with Teflon screwcaps. Samples for anoxic incubation were prepared and sampled using a sterile Aldrich® AtmosBag two-hand glove bag under nitrogen atmosphere. A mass (12 g) of end-member mixed samples were mixed with ultrapure water (Barnstead™ Easypure™ RoDi, Thermo Scientific) at a solid-to-solution ratio of 1:4 and equilibrated for 48 h in the dark at room temperature after shaking at 100 rpm for one hour. River water from the Jungnang River, a tributary of Seoul's Han River (37°40'16"N, 127°04' 47"E), was used as inoculum for microbial incubation. Before incubation, all artificial sediment samples were spiked with 3% (v/v) of the prepared inoculum, and a sufficient amount (1%, v/v) of nutrients (NH_4NO_3 and K_2HPO_4 at 10 mM) was added to each sample to avoid nutrient limitations during the incubation. The low inoculum-to-sample ratio had a negligible effect on the final OC concentrations of the end member mixtures (<1%) and on the molecular signature. Therefore, we concluded that the concentration and signature

of the inoculum could be safely ignored. Finally, the samples in oxic and anoxic conditions were incubated in the dark at 25 °C for 60 days (Guenet et al. 2014; Navel et al. 2012). Samples were collected for sampling on day 0 and day 60, with "day 0" corresponding to the day when the samples were inoculated. Degradation experiments were carried out in duplicate.

The sampling was performed as follows. First, samples were taken from the incubator, and the overlying water was carefully removed so as not to disturb the sediment. The artificial sediment samples were then centrifuged at 5000 rpm for 20 min to remove the porewater. Finally, the porewater-free sediment samples were freeze-dried, ground, and homogenized for further analyses. All the analyses were performed on both replicates except for the LDI FT-ICR MS where both replicates were carefully mixed in order to obtain a representative sample for the different modalities. Total organic carbon (TOC) contents of sediments were measured using an elemental analyzer coupled with an isotope ratio mass spectrometer (EA-IRMS; EuroEA-Isoprime IRMS, GV instruments, UK) for all samples in order to estimate the percentage of removal or production of OC after the 60 days of incubation (Supplementary Material, Table A.1).

2.2. Laser desorption ionization Fourier transform ion cyclotron resonance mass spectrometry (LDI FT–ICR MS)

Molecular analyses were performed with a (-) LDI solariX 2XR FT ICR mass spectrometer (Bruker Daltonic, Bremen, Germany) in Mass Spectrometry Based Convergence Research Center at Kyungpook National University. The instrument was equipped with a 7 T refrigerated actively shielded superconducted magnet and a dual-mode ESI/matrix-assisted laser desorption/ionization ion source with a frequency-tripled Nd:YAG (neodymium-doped yttrium aluminum garnet) laser emitting at 355 nm. Briefly, between 2 and 5 μg of freeze-dried artificial sediment samples were directly loaded onto preplaced double-sided tape on a MALDI (matrix-assisted laser desorption/ionization) plate. Before analysis, the plate was dried under

vacuum for 2 hours. The broadband spectra were acquired between *m*/*z* 100 and 1000, with a 4MW free induction decays (2 Ω), and 300 spectra were averaged to improve the signal-to-noise ratio. For data processing, only peaks with an S/N ratio of ≥ 4 were considered. A detailed description of the analytical method is given in Solihat et al. (2019).

Molecular formulae were assigned to peaks in the mass range of *m/z* 200-600 with a mass error range of ± 1ppm. Molecular formulae were identified considering the following elemental combinations: $^{12}C_{0-\infty}{}^{1}H_{0-\infty}{}^{16}O_{0-\infty}{}^{14}N_{0-5}{}^{32}S_{0-2}$. Only the formulae presented the following elemental ratio criteria, $0.3 \leq H/C \leq 2.25$, $O/C < 1.2$, $N/C < 0.5$, and $S/C < 0.2$, and the double bond equivalent rule (i.e., $DBE = 1/2(2C–H+N) \geq 0$) was considered (Koch et al. 2007). Several selected indices, including intensity-weighted average (wa) molecular masses, elemental ratios, DBE, AI_{mod} (modified aromatic index), and MLB_L (molecular lability boundary for labile contributions) were also calculated (D'Andrilli et al. 2015; Koch and Dittmar 2006). Finally, the assigned molecular formulae were examined using the van Krevelen diagram and were categorized into eight different compound classes (Supplementary Material, Table A.2) (Derrien et al. 2017; Kim et al. 2003).

2.3. Thermally assisted hydrolysis and methylation (THM) gas chromatography-mass spectrometry (THM–GC–MS)

THM–GC–MS analyses were performed according to Jeanneau et al. (2014). Briefly, we introduced between 0.3 mg (algae) and 5 mg (soil) of freeze-dried solid residue into an 80 µL aluminum reactor with an excess of solid tetramethylammonium hydroxide (ca. 10 mg). The THM reaction was performed on-line using a vertical micro-furnace pyrolyzer PZ-2020D (Frontier Laboratories, Japan) operating at 400 °C. The products of this reaction were injected into a gas chromatograph GC-2010 (Shimadzu, Japan) equipped with a SLB 5MS capillary column in the split mode (60 m × 0.25 mm ID, 0.25 µm film thickness). The temperature of the transfer line was 321°C, and the temperature of the injection port was 310 °C. The oven

was programmed to maintain an initial temperature of 50 °C for 2 minutes, then rise to 150 °C at 15 °C min^{-1}, and then rise to 310 °C at 3 °C min^{-1} where it stayed for 14 minutes. Helium was used as the carrier gas at a flow rate of 1.0 ml/min. Compounds were detected using a QP2010+ mass spectrometer (Shimadzu, Japan) operating in full scan mode. The temperature of the transfer line was set at 280 °C, the ionization source at 200 °C, and molecules were ionized by electron impact using an energy of 70 eV. The list of analyzed compounds and *m*/*z* ratios used for their integration are given in the Supplementary Material (Table A.2). Compounds were identified based on their full-scan mass spectra by comparison with the NIST library and with published data (Nierop and Verstraten 2004; Nierop et al. 2005).

The target compounds (i.e., 136 biomarkers) were classified into eight chemical families: small organic acids (SOAc), phenolic compounds (PHE) including lignin and tannin markers, carbohydrates (Car), low molecular weight fatty acids (LMWFA), high molecular weight fatty acids (HMWFA), fatty alcohols (Falcohol), chlorophyll markers (Phytol) including phytol and neophytadiene, and N-containing compounds (Ncompound). The peak area of the selected *m*/*z* (mass/charge) for each compound was integrated and corrected by a mass spectra factor calculated as the reciprocal of the proportion of the fragment used for the integration and the entire fragmentogram provided by the NIST library (Supplementary Material, Table A.3) (Denis et al. 2017; Jeanneau et al. 2018). The proportion of each compound class was calculated by dividing the sum of the areas of the compounds in this class by the sum of the peak areas of all analyzed compounds expressed as a percentage.

2.4. Statistical analyses

All the statistical analyses were performed with R (version 3.4.3) using the packages Vegan (Vegan 2.4-1) and FactoMineR.

2.4.1. LDI FT–ICR MS data

248 The Bray-Curtis dissimilarity matrix was computed for the whole set of the LDI FT–
249 ICR MS data (Supplementary Material, Table A.4 and A.5) to quantify the intra- and inter-
250 variability of the samples (Bray and Curtis 1957). Principal coordinates analysis (PCoA) was
251 then performed based on this dissimilarity matrix.

252 *2.4.2. THM–GC–MS data*

253 A first principal component analysis (PCA) was performed using the relative
254 proportions of the 136 biomarkers as variables, which allows the direct comparison of the
255 different samples without the concentration effect (Supplementary Material, Table A.6 and
256 A.7). This PCA allows identification of the correlated variables based on a modulus of the
257 Pearson coefficient > 0.8. When the two variables were correlated, the least abundant was
258 removed. Then a second PCA was performed. The variables with a correlation lower than 0.5
259 with the two first factors were removed, resulting in a new set of 67 variables. A third PCA
260 and the associated hierarchical ascendant classification (HAC) were calculated. A last PCA
261 and HAC were performed using specific microbial biomarkers (i.e., microbial FA: $n\mathrm{C}_{12:0}$,
262 $n\mathrm{C}_{13:0}$, $n\mathrm{C}_{14:0}$, $a\mathrm{C}_{15:0}$, $n\mathrm{C}_{15:0}$, $b\mathrm{rC}_{16:0}$, $n\mathrm{C}_{16:1}$, $n\mathrm{C}_{17:0}$, $n\mathrm{C}_{18:1}$ (2 isomers), and $n\mathrm{C}_{19:1}$) in order to
263 explore the role of the microbial activity during biodegradation. $n\mathrm{C}_{16:0}$ and $n\mathrm{C}_{18:0}$ were not
264 considered since these biomarkers are produced by the THM of algae and derive from higher
265 plant inputs, respectively.
266

3. Results and discussion

All the detailed results of LDI FT–ICR MS and THM–GC–MS are presented in Supplementary Material (Tables A.4-7),

3.1. Identification of the biodegradation-induced changes in the pure end-member artificial sediments

At day 0, no differences were observed based on the H/C and O/C ratios, but a clear distinction was observed for the distribution between the CHO, CHON, CHOS, and CHONS elemental formulae, common indices, and compound classes between both pure artificial sediments (S:A, 100:0 and S:A, 0:100) (Table A4-5). S:A, 100:0 mainly contained carbon-rich and heavily carboxylated compounds with a part of them rich in nitrogen (e.g., CHO of 55.2% and 39.3% and CHON of 33.6% and 38.4% in oxic and anoxic conditions respectively). By contrast, S:A, 0:100 exclusively consisted of CHO compounds (e.g., 98.9% and 96.5% in oxic and anoxic conditions respectively). Higher values of DBE and AI_{mod} and a much lower value for the MLB_L for S:A, 0:100 than for S:A, 100:0 indicated the presence of highly aromatic and unsaturated compounds in the composition of the algae and the near absence of labile compounds. This was supported by the identification and distribution of the compounds classes as the S:A, 0:100 mainly consisted of unsaturated hydrocarbons (e.g., 36.3% and 37.5% for oxic and anoxic conditions, respectively), lignins/CRAM (e.g., 30.7% and 30.4% for oxic and anoxic conditions, respectively) and condensed aromatic structures (CAS, e.g., 30.1% and 27.2% for oxic and anoxic conditions, respectively) (Fig. 1). Algae material is commonly associated with labile material, however, it was also demonstrated that this kind of material can be characterized by a high amount of hydrocarbons (Youngblood et al. 1971), lignins (Alzate-Gaviria et al. 2020; Martone et al. 2009) and by biopolymers such as the algaenans, which represent the major constituent of the cell walls of green algae, for instance (Derenne et al. 1992; Gelin et al. 1996). S:A, 100:0 also presented a distribution in compounds class rich in

292 CAS (e.g., 51.2% and 37.2% for oxic and anoxic conditions, respectively) and lignins/CRAM
293 (e.g., 31.1% and 38.2% for oxic and anoxic conditions, respectively). However, the rest of the
294 distribution consisted of lipids (e.g., 7.1% and 7.3% for oxic and anoxic conditions,
295 respectively), unsaturated hydrocarbons and/or tannins (e.g., ~5%), and a small amount of
296 labile material such as proteins (e.g., ~3%) and carbohydrates and amino sugars (e.g, ~2%)
297 (Fig. 1).

298 After 60 days of incubation, the main observed differences were related to the
299 distribution in compound classes. A decrease of the highest molecular weight compounds (i.e.,
300 CAS and Lignins/CRAM) in S:A, 0:100 was observed in favor of an increase of the percentage
301 of unsaturated hydrocarbons of 10.8 and 21.7 points with values reaching 47.1% and 592.2%
302 for oxic and anoxic conditions, respectively (Fig. 1). A slight increase in labile compounds was
303 also observed. Regarding the S:A, 100:0, the few changes were mainly observed in oxic
304 conditions, with a decrease in the observed percentage of the CAS (e.g., from 51.2% to 38.9%
305 at day 0 and day 60, respectively). In parallel, a slight increase in the percentage of the
306 lignins/CRAM and labile compounds was also noted for both oxygen conditions. Classically,
307 biodegradation is associated with a rapid loss of low molecular weight (LMW) compounds
308 (Hansen et al. 2016; Wetzel 2001). However, in the present study, the results suggest
309 preferential biodegradation of the high molecular weight (HMW) compounds associated with
310 conversion into lower molecular weight compounds (Curtis-Jackson et al. 2009; Hach et al.
311 2020; Liu et al. 2019; Moran and Zepp 1997). These observations agree with the paradigm in
312 which all organic molecules could be biodegradable irrespective of their recalcitrance if
313 favorable physical, chemical, and biological factors are present (Kleber 2010). This
314 observation can be also the result of two-step processes. As it was previously observed in the
315 literature, LMW compounds could have been consumed primarily generating a rapid loss of
316 labile and LMW materials followed by the consumption of HMW compounds (e.g., CAS and

317 lignins/CRAM) and their transformations in LMW compounds (D'Andrilli et al. 2019; Hansen
318 et al. 2016). Unfortunately, the sampling design does not allow us to identify which processes
319 (one or two steps processes) occurred.
320 Regarding the biomarker distributions, two distinctive fingerprints were identified between the
321 2 pure end-member artificial sediments but closely the same irrespective of the oxygen
322 condition (Fig. 2). In S:A, 100:0, the most abundant chemical family was HMWFA with
323 aliphatic side chain containing 20 and more C atoms (60.6 ± 3.3% and 60.0 ± 7.4% for oxic
324 and anoxic conditions, respectively). These HMWFA included linear n-alkanoic acids from *n*-
325 $C_{20:0}$ to *n*-$C_{30:0}$ with an even-over-odd predominance characteristic of plant-derived inputs
326 (Eglinton and Hamilton 1967), linear ω-hydroxyacids and α,ω-diacids from *n*-C_{16} to *n*-C_{26},
327 10,16-dihydroxy$C_{16:0}$ and 9,10,18-trihydroxy $C_{18:0}$ characteristic of plant-derived aliphatic
328 biopolymers cutin and suberin (Armas-Herrera et al. 2016; Kolattukudy 2001). The main
329 molecules were 9,10,18-trihydroxy$C_{18:0}$ (21.4 ± 0.9% and 14.5 ± 7.6% for oxic and anoxic
330 conditions, respectively) and ωOH-C22 (7.9 ± 0.7% and 10.7 ± 0.7% for oxic and anoxic
331 conditions, respectively), which indicated a higher proportion of suberin from roots than cutin
332 from leaves (Mueller et al. 2012) (Table A6-7). The second most abundant chemical family
333 was PHE produced by the THM of lignins and tannins (11.5 ± 0.0% and 11.7 ± 3.2% for oxic
334 and anoxic conditions, respectively). This chemical family was dominated by 3,4-
335 dimethoxybenzoic acid methyl ester and 3,4,5-trimethoxybenzoic acid methyl ester, which are
336 typical of the THM of woody plants (Challinor 1995) and applied to investigate the transfer
337 and reactivity of OM (Denis et al. 2017; Williams et al. 2016). The third chemical family was
338 LMWFA with 8.9 ± 0.4% and 11.4 ± 3.1% for oxic and anoxic conditions, respectively. This
339 chemical family includes n-alkanoic acids from *n*-$C_{8:0}$ to *n*-$C_{19:1}$, iso and anteiso $C_{15:0}$ and $C_{17:0}$,
340 iso $C_{14:0}$ and $C_{16:0}$ and n-alkenoic acids *n*-$C_{16:1}$, *n*-$C_{18:1}$ and *n*-$C_{19:1}$. The LMWFA with less than
341 13 C atoms can be derived from microbial or plant-derived inputs, while the LMWFA with

more than 13 C atoms are known as phospholipid fatty acids and are microbial biomarkers (Frostegård et al. 1993) except for *n*-$C_{16:0}$ and *n*-$C_{18:0}$, which can derive from plant-derived inputs. In S:A, 0:100, the most abundant chemical family was LMWFA with 67.8 ± 3.1% and 61.3 ± 3.8% for oxic and anoxic conditions, respectively. The distribution of the compounds was different from that analyzed in S:A, 100:0, with a large predominance of *n*-$C_{16:0}$ (19.3 ± 0.2% and 22.3 ± 0.3% for oxic and anoxic conditions, respectively) and a large proportion of *n*-$C_{16:2}$ (12.1 ± 2.3% and 9.5 ± 0.7% for oxic and anoxic conditions, respectively) and *n*-$C_{18:2}$ (32.9 ± 2.3% and 25.7 ± 2.8% for oxic and anoxic conditions, respectively). The second most abundant chemical family was the chlorophyll biomarkers with two compounds: phytol and neophytadiene. They represented 18.3 ± 3.2% and 21.5 ± 7.8% of oxic and anoxic conditions, respectively. Finally, the third chemical family was composed of N-containing compounds, which represented 10.6 ± 0.1% and 13.6 ± 3.2% (i.e., for oxic and anoxic conditions, respectively). Among this family, 1,3-dimethyluracil was the dominant compound (4.3 ± 0.6% and 7.3 ± 1.1% for oxic and anoxic conditions, respectively).

After 60 days of incubation, the characteristic chemical fingerprints of each pure end-member artificial sediments remained the same, and no significant differences were observed (Fig. 2).

3.2. Identification of the biodegradation-induced changes in mixed samples

The mixed artificial sediments (e.g., S:A, 75:25; S:A, 50:50 and S:A, 25:75) did not show notable differences in their molecular profile at day 0 (Table A.4- 5). A slight increase for the H/C_{wa} was observed compared to the end members with values of ~1.1 instead of 0.8 or 0.9, suggesting a lower unsaturation for these samples that was confirmed by the values of DBE, which are much lower than for both pure end-member artificial sediments (e.g., values ranged from 10.8 to 12.6 irrespective of the oxygen conditions). Likewise, the values of AI_{mod}> 0.5 and inferior to both pure end-member artificial sediments demonstrated the occurrence also

of less aromatic compounds. The elemental formula distributions of CHO and CHON are also quite close to each other, whatever the proportions of algae; even so, a slightly higher proportion of CHON formula compounds is observed in anoxic conditions for the S:A, 25/75 mixed sediment which reaches 49.2% for instance. The percentages of formulae with sulfur (i.e., CHOS and CHONS) were higher than for either end members with values ranging from ~10% to ~17% for CHOS and ~7% to 14.3% for CHONS. Regarding the distribution in compound classes, similarities in values were also observed (Fig. 1). The two main groups of compound classes were lignins/CRAM and CAS with percentages ranging from 38.6% to 44.2% and 22.2% to 30.2% respectively, followed by lipids and unsaturated hydrocarbons with percentages ranged between 9% and 17.9%. Proteins and carbohydrates and aminosugars occurred at less than 5%, respectively. This distribution was also reflected in the MLB_L index (percentage of labile material), which reaches values 1.5- to 7-fold those observed for the soil or pure algae artificial sediment, respectively (Table A.4 and A.5).

After 60 days of incubation, each mixed artificial sediment displayed a unique molecular profile compared to the initial according to its ratio of end-members and/or its oxygen condition. S:A, 50:50, irrespective of the oxygen conditions, strictly showed the same distribution in compounds class, suggesting a homogeneous effect of the biodegradation on the whole pool of OM an. A similar observation was made for S:A, 75:25 in oxic conditions. By contrast, molecular changes were observed in S:A, 25:75 for both oxygen conditions and specifically for S:A, 75:25 in anoxic conditions (Fig. 1). In S:A, 75:25, a decrease of the CAS and lignin/CRAM was noted in favor of the unsaturated hydrocarbons becoming, thus, the main compound class (i.e., 33.7%). For S:A, 25:75, similar changes were also observed, however, the lignin/CRAM compound class remained the main one (i.e., values of 39% and 33% for oxic and anoxic conditions, respectively). Similar changes to the changes observed for the end-member in higher proportion would have been expected, however, results displayed different

trends as 3 different scenarios of biodegradation according to the mixing ratios were observed (e.g., no changes or homogeneous changes for all types of compounds, consumption of LMW compounds associated to production of LMW compounds and preferential degradation of one type of HMW compounds). These differences and similarities in the compound distribution for the mixed samples suggest the occurrence of underlying mechanisms.

At day 0, the biomarker distribution ~~of biomarkers~~ into chemical families illustrated a gradual modification of the biomarker distribution induced by the mixing of end-members (Fig. 2). This gradual modification was characterized by the progressive increase in the proportion of LMWFA from 24.0 ± 5.2% (S:A,75:25; 26.3 ± 6.0% and 21.6 ± 4.7% in oxic and anoxic conditions, respectively) to 55.4 ± 3.8% (S:A, 25:75; 57.8 ± 4.6% and 53.0 ± 0.2% in oxic and anoxic conditions, respectively). An increase in the proportion of chlorophyll biomarkers was also observed with the increase of algae proportions with values from 3.0 ± 1.3% (S:A, 75:25, 3.8 ± 1.4% and 2.2 ± 0.9% in oxic and anoxic conditions, respectively) to 11.0 ± 3.5% (S:A, 25:75, 11.0 ± 1.4% and 11.0 ± 5.8% in oxic and anoxic conditions, respectively). At the same time, the proportion of HMWFA decreased from 45.0 ± 6.4% (S:A, 75:25; 41.6 ± 7.5% and 48.3 ± 4.6% in oxic and anoxic conditions, respectively) to 19.6 ± 3.9% (S:A, 25:75; 18.5 ± 4.1% and 20.6 ± 4.8% in oxic and anoxic conditions, respectively). The PHE proportion also decreased regularly from 9.5 ± 1.1% (S:A, 75:25; 8.8 ± 0.2% and 10.2 ± 1.0% in oxic and anoxic conditions, respectively) to 2.3 ± 0.4% (S:A, 75:25; 2.0 ± 0.2% and 2.6 ± 0.3% in oxic and anoxic conditions, respectively).

At day 60, various changes were observed in the distribution of biomarkers. The most significant changes were observed for S:A, 75,25, and S:A, 50:50, and specifically in anoxic conditions, where a significant (p-value < 0.05) diminution was observed for almost all the types of chemical families. By contrast, an increase in the proportion of LMWFA was observed for all mixing ratios and oxygen conditions, but this increase was significant only for S:A,

75;25 and S:A, 50:50 in anoxic conditions. Regarding S:A, 25:75 only the diminution of SOAc and Ncompound were significant.

3.3. Factors controlling the biodegradation

3.3.1. Source mixing factor

In order to understand the role and the weight of the factor "source", a PCoA was performed based on the Bray-Curtis dissimilarity matrix computed all the FT–ICR MS parameters (Fig. 3). Unfortunately, the ordination did not show any clear distinction either according to the sources or mixing of sources and/or the incubation time. Although FT–ICR MS analysis has emerged as a reliable tool for the in-depth molecular characterization of complex mixtures as OM with the capacity of identifying thousands of molecules per sample and assigning associated elemental formulae with a high level of confidence (Repeta 2015; Stubbins and Dittmar 2014), this technique can also present some inherent limitations. The main limitations of the FT–ICR MS tool relate to the inconsistent ionization efficiency for different sample matrices, potentially leading to a bias of detection toward certain groups of compounds or even to un-characterization of material (Blackburn et al. 2017; D'Andrilli et al. 2020; Dittmar et al. 2008; Hawkes et al. 2019; Mopper et al. 2007; Patriarca et al. 2020). In the present study, it is noticed the number of assigned formulae decreased gradually with the increase of the algae end-member, which could be assimilated to lower efficiency of the ionization for this kind of matrix (Table A.4 and A.5) (Blackburn et al. 2017; Kew et al. 2018). A lower ionization efficiency and preferential ionization for some group of compounds might constrain the data interpretation and make it harder for disentangling the complexity of the OM molecular composition (Derrien et al. 2019a; Hawkes et al. 2018). This could be one of the reasons for the failure of the ordination to identify sub-groups according to the sources, oxygen conditions, and/or time of incubations. Another reason could be related to the non-discriminatory character of the data. FT-ICR MS is a technique able to identify with high

accuracy hundreds to several thousands of ions with an *m*/*z* range typically from 200 to 1000 Da. However, this level of sensitivity is not that discriminant for observing an ordination between our set of samples.

By contrast, we clearly identified an effect of the factor "source" through the use of the biomarkers. The PCA based on the distribution of the 67 variables displayed a clear separation on ~~axis~~ PC1 according to the proportion of algae (Fig. 4). The HAC performed on the results of this latter PCA identified 4 groups. The 2 pure artificial sediments at day 0 and day 60 were grouped with their respective endmember sample in two different groups (Groups 1 and 3). The biomarker fingerprint modifications induced by the mixing of end-members were fairly well illustrated by the projection of the samples at day 0 on PC1, representing 62.7% of the variance of the dataset. They corresponded almost exactly to the theoretical points calculated via the end-member mixing approach (Fig. 4). The HAC grouped S:A, 75:25 at day 0 samples with the S:A, 100:0 (Group 3) and the rest of the mixed samples (S:A, 50:50 and 25:75) from day 0 as a distinct group (Group 2). The last group identified by the HAC consisted of all three S:A mixed samples from day 60 (Group 4). This group was characterized by proportions of *n*-$C_{14:0}$, *n*-$C_{15:0}$, *n*-$C_{16:0}$, *a*$C_{15:0,}$ and *n*-$C_{18:0}$ FA higher than the mean of the samples and by proportions of N-containing compounds, succinic and fumaric acids, *n*-$C_{18:1}$, *n*-$C_{18:2}$, *n*-$C_{16:2}$ FA, and α,ω-diacid *n*-$C_{9:0}$ lower than the mean of the samples. 60 days' incubation resulted in a specific decrease in the proportion of compounds that were specific to algae namely N-containing compounds and di-unsaturated FA. However, this decrease was not associated with an increase in soil-specific markers such as HMWFA or PHE whose proportions tend to decrease or to remain stable during the incubation (Fig. 2). This decrease was significant (Wilcoxon test) only for PHE for S:A, 75:25, and 50:50. In the same time, the proportion of microbial FA increased, which could be interpreted as stimulation of microbial biomass and therefore the occurrence of positive priming effects (Guenet et al. 2014).

467 *3.3.2. Oxygen factor*

468 Oxygen is one of the most important reactants in biogeochemical cycles as it impacts
469 the redox potential of the environment as well as the energetic situation of the microorganisms
470 (Brune et al. 2000). Therefore, its occurrence or absence may affect the biodegradation
471 processes and pathways. In the molecular profiles obtained by LDI FT–ICR MS, the main
472 differences were observed in S:A, 25:75, S:A, 75:25, and S:A, 0:100. The absence of oxygen
473 led to a higher production of unsaturated hydrocarbons of 1.5 to ~3 times higher at day 60 than
474 at day 0 with values from 12.0% to 33.7% and from 17.9% to 28.3% for the S:A, 25:75 and
475 S:A, 75:25 samples, respectively (Fig. 1 and Table A.5). In parallel, for the same samples, a
476 higher distribution was noticed in labile compounds after biodegradation than in oxic
477 conditions. These observations suggest a preferential biodegradation through the conversion of
478 HMW molecules into smaller compounds. By contrast, no differences were observed for the
479 distribution in biomarkers (Fig. 2). This was also confirmed with the PCA as the oxic and
480 anoxic samples are gathered together with no exceptions (Fig. 4). From our results, it seems
481 difficult to state on the effect of the oxygen condition on the observed biodegradation pathways.

482 *3.4. Behind the chemical mechanisms of biodegradation*

483 In order to further investigate the potential stimulation of the microbial biomass and
484 determine if there was a modification of the composition of the microbial community, the
485 distribution of microbial FA (e.g., FA with a low molecular weight (< $C_{19:0}$) except for $C_{16:0}$
486 and $C_{18:0}$) was investigated using a PCA and a HAC, resulting in four groups depicted by grey
487 areas in Fig. 5. At day 0, the distribution of microbial FA in soil was modified by the addition
488 of algae. The evolution of this distribution was almost regular along the segment formed by the
489 end members. For algae, samples from days 0 and 60 remained in the same group (Group 1),
490 which highlighted that the distribution of FA remained almost stable during the incubation. On
491 the contrary for the soil, samples from day 60 were plotted in a distinct group (Group 3). This

492 indicates a modification of the distribution of microbial FA during the experiment, which could
493 be interpreted as a modification of the composition of the microbial community (Frostegård et
494 al. 1993). The S:A mixed samples at day 60 were also classified as a specific group (Group 4).
495 The direction of the modifications of the distribution of microbial FA was almost orthogonal
496 (i) to the segment formed by the end members and (ii) to the direction of the modifications in
497 the soil during the experiment. Consequently, these changes in the distribution of FA were not
498 only the result of the mixture but were also due to the adaptation of the composition of
499 microbial communities to the mixture of soil and algae.

500 A second point is that the Euclidean distance between day 0 and 60 for the different
501 S:A ratios seems to increase with the proportion of algae from 2.9 ± 0.9 (S:A, 75:25) to 3.9 ±
502 0.3 (S:A, 50:50) and 4.7 ± 0.3 (S:A, 25:75). The number of experimental replicates was not
503 sufficient to test the significance of this increase. However, it could suggest that the magnitude
504 of the modification of the composition of microbial communities increased with the proportion
505 of algae added to the soil. Moreover, S:A mixed samples at day 60 were grouped without clear
506 differentiations of mixture ratios, which could indicate that the modification of the microbial
507 communities was independent of the S:A ratio. Finally, this group of S:A mixed samples from
508 day 60 were characterized by proportions of *n*-$C_{12:0}$ and *n*-$C_{14:0}$ higher than the average and
509 proportion of *n*-$C_{18:1}$ (isomer 1), *n*-$C_{17:0}$ and *n*-$C_{19:1}$ lower than the average. Moreover, *n*-$C_{18:1}$
510 (isomer 1) correlated with *i*$C_{17:0}$. The differences between the average proportion in group 4
511 and the average proportion in the entire dataset were significant for *i*$C_{17:0}$ (p-value < 0.001).
512 This group may then be associated with a decrease in the proportion of terminally branched FA
513 (*i*$C_{17:0}$) that has been proposed as a marker of Gram-positive bacteria (Willers et al. 2015).
514 These results could signify that this microbial group was disadvantaged by the mixing of soil
515 with algae.
516

4. Conclusion

This study aimed at gaining insights into the biodegradation pathways and molecular modifications of sedimentary organic matter, as well as to fathom the underlying mechanisms via a laboratory experiment. The FT–ICR MS analysis allowed us to identify the group of compounds preferentially degraded during early microbial diagenesis. In both pure end-members, CAS and lignins/CRAM were identified as the molecules the most affected by biodegradation. For the mixed artificial sediments (i.e., S:A, 75:25, S:A, 50:50, and S:A, 25:75), distinct biodegradation alterations emerged for each ratio, underscoring the potent influence of the "source" factor. The divergent shifts in compositional changes for different mixing ratios post-incubation also hint at the potential involvement of underlying mechanisms, such as priming effects. Notably, with the present study design, no discernible correlation was established between the proportions of labile material and the intensity of priming effects. Furthermore, the combination of the biomarker and molecular analyses allowed us to suggest the capability of the microbial communities to adapt or shift in response to the varying types and proportions of organic matter sources, facilitating the biodegradation of diverse materials. However, additional studies and complementary qualitative analyses are imperative to test this hypothesis conclusively. Nevertheless, this latter observation underscores the compelling need to delve into and elucidate the intricate interplay between microbial communities and organic matter. Addressing this challenge necessitates a holistic analytical approach, one that combines organic geochemistry and meta-omic methods. This holistic approach, as underlined by Bianchi and Ward (2019), would enable the identification of both the composition and function of microbial communities. While this study indeed stems from a controlled laboratory experiment, resulting in the formulation of questions and hypotheses for future testing, it fundamentally demonstrates the intrinsic significance of chemical, biological, and environmental factors in shaping the reactivity of OM.

Acknowledgments

This work was supported by a National Research Foundation of Korea (NRF) grant [No. 2017R1D1A1B033546, 2017] funded by the Korean government (MSIP). The authors thank Dr. Yunju Cho for handling the LDI FT–ICR MS analyses. THM-GCMS analyses were performed through the support of the Condate Eau - OSUR analytical platform of Rennes University.

Data Availability Statement

The data that support this study are available in the article and accompanying online supplementary material.

Conflict of Interest statement

The authors declare no conflicts of interest.

Declaration of Funding

The funding of this work was the National Research Foundation of Korea (NRF) grant [No. 2017R1D1A1B033546, 2017] from the Korean government (MSIP).

Figure' captions

562 **Fig. 1** Distribution in compounds classes and elemental formulas of all the artificial sediments
563 for both oxygen conditions (i.e., oxic and anoxic). Characteristics of compound classes are
564 presented in Table A.2.
565 **Fig. 2** Relative proportions of the chemical families identified by the THM–GC–MS analysis
566 of the end members at t = 0 day and t = 60 days in all the artificial sediments for both oxygen
567 conditions (i.e., oxic and anoxic). Uncertainties are the standard deviation of two experimental
568 replicates. Asterisks was added on data where a significant difference (p-value < 0.05) is
569 observed between day 0 and day 60.
570 **Fig. 3** Principal coordinate analysis ordination of the Bray-Curtis dissimilarity matrix
571 computed for the LDI FT–ICR MS data.
572 **Fig. 4** Principal component analysis performed with the distribution of biomarker (67). Purple
573 pentagons are the theoretical points of the S:A mixed samples calculated using an end-member
574 mixing approach. Grey shapes highlight the groups identified by the hierarchical analysis
575 classification.
576 **Fig. 5** Principal component analysis performed with the distribution of microbial fatty acids
577 biomarker (11). Grey shapes highlight the groups identified by the hierarchical analysis
578 classification.

579

580 **References**

581 Alzate-Gaviria, L., Domínguez-Maldonado, J., Chablé-Villacís, R., Olguin-Maciel, E., Leal-
582 Bautista, R.M., Canché-Escamilla, G., Caballero-Vázquez, A., Hernández-Zepeda, C.,
583 Barredo-Pool, F.A., Tapia-Tussell, R., 2020. Presence of polyphenols complex aromatic
584 "lignin" in Sargassum spp. from Mexican Caribbean. *J Mar Sci Eng* **9**, 6.
585 Armas-Herrera, C.M., Dignac, M., Rumpel, C., Arbelo, C.D., Chabbi, A., 2016. Management
586 effects on composition and dynamics of cutin and suberin in topsoil under agricultural
587 use. *Eur J Soil Sci* **67**, 360–373.
588 Arndt, S., Jørgensen, B.B., LaRowe, D.E., Middelburg, J.J., Pancost, R.D., Regnier, P., 2013.
589 Quantifying the degradation of organic matter in marine sediments: A review and

590 synthesis. *Earth Sci Rev* **123**, 53–86.
591 https://doi.org/10.1016/J.EARSCIREV.2013.02.008
592 Aubriet, F., Carré, V., 2019. Fourier transform ion cyclotron resonance mass spectrometry
593 and laser: A versatile tool. *Fundamentals and Applications of Fourier Transform Mass*
594 *Spectrometry* 281–322. https://doi.org/10.1016/B978-0-12-814013-0.00010-7
595 Bengtsson, M.M., Attermeyer, K., Catalán, N., 2018. Interactive effects on organic matter
596 processing from soils to the ocean: are priming effects relevant in aquatic ecosystems?
597 *Hydrobiologia*. https://doi.org/10.1007/s10750-018-3672-2
598 Bianchi, T.S., 2011. The role of terrestrially derived organic carbon in the coastal ocean: a
599 changing paradigm and the priming effect. *Proc Natl Acad Sci U S A* **108**, 19473–19481.
600 https://doi.org/10.1073/pnas.1017982108
601 Bianchi, T.S., Ward, N.D., 2019. Editorial: The Role of Priming in Terrestrial and Aquatic
602 Ecosystems. *Front Earth Sci (Lausanne)* **7**. https://doi.org/10.3389/feart.2019.00321
603 Blackburn, J.W.T., Kew, W., Graham, M.C., Uhrin, D., 2017. Laser desorption/ionization
604 coupled to FTICR mass spectrometry for studies of natural organic matter. *Anal Chem*
605 **89**, 4382–4386.
606 Bowen, S.R., Gregorich, E.G., Hopkins, D.W., 2009. Biochemical properties and
607 biodegradation of dissolved organic matter from soils. *Biol Fertil Soils* **45**, 733–742.
608 Bray, J.R., Curtis, J.T., 1957. An Ordination of the Upland Forest Communities of Southern
609 Wisconsin. *Ecol Monogr* **27**, 325–349. https://doi.org/10.2307/1942268
610 Briand, M.J., Bonnet, X., Goiran, C., Guillou, G., Letourneur, Y., 2015. Major Sources of
611 Organic Matter in a Complex Coral Reef Lagoon: Identification from Isotopic
612 Signatures (δ(13)C and δ(15)N). *PLoS One* **10**, e0131555.
613 https://doi.org/10.1371/journal.pone.0131555
614 Brune, A., Frenzel, P., Cypionka, H., 2000. Life at the oxic–anoxic interface: microbial
615 activities and adaptations. *FEMS Microbiol Rev* **24**, 691–710.
616 https://doi.org/doi:10.1111/j.1574-6976.2000.tb00567.x
617 Challinor, J.M., 1995. Characterisation of wood by pyrolysis derivatisation—gas
618 chromatography/mass spectrometry. *J Anal Appl Pyrolysis* **35**, 93–107.
619 Choi, H.-M., Yang, K.-C., 2012. Classification of tree species using high-resolution
620 QuickBird-2 satellite images in the valley of Ui-dong in Bukhansan National Park. *J*
621 *Ecol Environ* **35**, 91–98.
622 Curtis-Jackson, P.K., Massé, G., Gledhill, M., Fitzsimons, M.F., 2009. Characterization of
623 low molecular weight dissolved organic nitrogen by liquid chromatography-electrospray
624 ionization-mass spectrometry. *Limnol Oceanogr Methods* **7**, 52–63.
625 https://doi.org/doi:10.4319/lom.2009.7.52
626 D'Andrilli, J., Cooper, W.T., Foreman, C.M., Marshall, A.G., 2015. An ultrahigh-resolution
627 mass spectrometry index to estimate natural organic matter lability. *Rapid*
628 *Communications in Mass Spectrometry* **29**, 2385–2401.
629 https://doi.org/10.1002/rcm.7400
630 D'Andrilli, J., Fischer, S.J., Rosario-Ortiz, F.L., 2020. Advancing Critical Applications of
631 High Resolution Mass Spectrometry for DOM Assessments: Re-Engaging with Mass
632 Spectral Principles, Limitations, and Data Analysis. *Environ Sci Technol* **54**, 2020.
633 https://doi.org/10.1021/acs.est.0c04557
634 D'Andrilli, J., Junker, J.R., Smith, H.J., Scholl, E.A., Foreman, C.M., 2019. DOM
635 composition alters ecosystem function during microbial processing of isolated sources.
636 *Biogeochemistry*. https://doi.org/10.1007/s10533-018-00534-5
637 Denis, M., Jeanneau, L., Petitjean, P., Murzeau, A., Liotaud, M., Yonnet, L., Gruau, G., 2017.
638 New molecular evidence for surface and sub-surface soil erosion controls on the

composition of stream DOM during storm events. *Biogeosciences* **14**, 5039–5051. https://doi.org/10.5194/bg-14-5039-2017

Derenne, S., Largeau, C., Berkaloff, C., Rousseau, B., Wilhelm, C., Hatcher, P.G., 1992. Non-hydrolysable macromolecular constituents from outer walls of Chlorella fusca and Nanochlorum eucaryotum. *Phytochemistry* **31**, 1923–1929. https://doi.org/10.1016/0031-9422(92)80335-C

Derrien, M., Lee, Y.K., Park, J.E., Li, P., Chen, M., Lee, S.H., Lee, S.H., Lee, J.B., Hur, J., 2017. Spectroscopic and molecular characterization of humic substances (HS) from soils and sediments in a watershed: comparative study of HS chemical fractions and the origins. *Environmental Science and Pollution Research* **24**, 16933–16945. https://doi.org/10.1007/s11356-017-9225-9

Derrien, M., Retelletti Brogi, S., Gonçalves-Araujo, R., 2019a. Characterization of aquatic organic matter: Assessment, perspectives and research priorities. *Water Res* **163**, 114908. https://doi.org/10.1016/J.WATRES.2019.114908

Derrien, M., Shin, K.H., Hur, J., 2019b. Assessment on applicability of common source tracking tools for particulate organic matter in controlled end member mixing experiments. *Science of The Total Environment* **666**, 187–196. https://doi.org/10.1016/j.scitotenv.2019.02.258

Derrien, M., Shin, K.-H.H., Hur, J., 2019c. Biodegradation-induced signatures in sediment pore water dissolved organic matter: Implications from artificial sediments composed of two contrasting sources. *Science of The Total Environment* **694**, 133714. https://doi.org/10.1016/j.scitotenv.2019.133714

Dittmar, T., Koch, B., Hertkorn, N., Kattner, G., 2008. A simple and efficient method for the solid-phase extraction of dissolved organic matter (SPE-DOM) from seawater. *Limnol Oceanogr Methods* **6**, 230–235. https://doi.org/10.4319/lom.2008.6.230

Eglinton, G., Hamilton, R.J., 1967. Leaf epicuticular waxes. *Science (1979)* **156**, 1322–1335.

Frostegård, Å., Tunlid, A., Bååth, E., 1993. Phospholipid fatty acid composition, biomass, and activity of microbial communities from two soil types experimentally exposed to different heavy metals. *Appl Environ Microbiol* **59**, 3605–3617.

Gelin, F., Boogers, I., Noordeloos, A.A.M., Sinninghe Damsté, J.S., Hatcher, P.G., De Leeuw, J.W., 1996. Novel, resistant microalgal polyethers: An important sink of organic carbon in the marine environment? *Geochim Cosmochim Acta*. https://doi.org/10.1016/0016-7037(96)00038-5

Gontikaki, E., Thornton, B., Huvenne, V.A.I., Witte, U., 2013. Negative priming effect on organic matter mineralisation in NE Atlantic slope sediments. *PLoS One* **8**, e67722.

Guenet, B., Danger, M., Abbadie, L., Lacroix, G., 2010a. Priming effect: bridging the gap between terrestrial and aquatic ecology. *Ecology* **91**, 2850–2861. https://doi.org/doi:10.1890/09-1968.1

Guenet, B., Danger, M., Harrault, L., Allard, B., Jauset-Alcala, M., Bardoux, G., Benest, D., Abbadie, L., Lacroix, G., 2014. Fast mineralization of land-born C in inland waters: first experimental evidences of aquatic priming effect. *Hydrobiologia* **721**, 35–44. https://doi.org/10.1007/s10750-013-1635-1

Guenet, B., Leloup, J., Raynaud, X., Bardoux, G., Abbadie, L., 2010b. Negative priming effect on mineralization in a soil free of vegetation for 80 years. *Eur J Soil Sci* **61**, 384–391.

Hach, P.F., Marchant, H.K., Krupke, A., Riedel, T., Meier, D. V., Lavik, G., Holtappels, M., Dittmar, T., Kuypers, M.M.M., 2020. Rapid microbial diversification of dissolved organic matter in oceanic surface waters leads to carbon sequestration. *Sci Rep* **10**, 13025. https://doi.org/10.1038/s41598-020-69930-y

Hansell, D.A., 2013. Recalcitrant dissolved organic carbon fractions.
Hansen, A.M., Kraus, T.E.C., Pellerin, B.A., Fleck, J.A., Downing, B.D., Bergamaschi, B.A., 2016. Optical properties of dissolved organic matter (DOM): Effects of biological and photolytic degradation. *Limnol Oceanogr* **61**, 1015–1032. https://doi.org/10.1002/lno.10270
Hawkes, J., Sjöberg, P.J.R., Bergquist, J., Tranvik, L., 2019. Complexity of dissolved organic matter in the molecular size dimension: insights from coupled size exclusion chromatography electrospray ionisation mass spectrometry. *Faraday Discuss*. https://doi.org/10.1039/C8FD00222C
Hawkes, J.A., Patriarca, C., Sjöberg, P.J.R., Tranvik, L.J., Bergquist, J., 2018. Extreme isomeric complexity of dissolved organic matter found across aquatic environments. *Limnol Oceanogr Lett* **3**, 21–30. https://doi.org/doi:10.1002/lol2.10064
Henrichs, S.M., 1992. Early diagenesis of organic matter in marine sediments: progress and perplexity. *Mar Chem* **39**, 119–149. https://doi.org/10.1016/0304-4203(92)90098-U
Herzsprung, P., von Tümpling, W., Wendt-Potthoff, K., Hertkorn, N., Harir, M., Schmitt-Kopplin, P., Friese, K., 2017. High field FT-ICR mass spectrometry data sets enlighten qualitative DOM alteration in lake sediment porewater profiles. *Org Geochem* **108**, 51–60. https://doi.org/https://doi.org/10.1016/j.orggeochem.2017.03.010
Jeanneau, L., Jaffrézic, A., Pierson-Wickmann, A.-C., Gruau, G., Lambert, T., Petitjean, P., 2014. Constraints on the sources and production mechanisms of dissolved organic matter in soils from molecular biomarkers. *Vadose Zone Journal* **13**.
Jeanneau, L., Rowland, R., Inamdar, S., 2018. Molecular fingerprinting of particulate organic matter as a new tool for its source apportionment: changes along a headwater drainage in coarse, medium and fine particles as a function of rainfalls. *Biogeosciences* **15**, 973–985. https://doi.org/10.5194/bg-15-973-2018
Kalbitz, K., Schmerwitz, J., Schwesig, D., Matzner, E., 2003. Biodegradation of soil-derived dissolved organic matter as related to its properties. *Geoderma* **113**, 273–291.
Kellerman, A.M., Kothawala, D.N., Dittmar, T., Tranvik, L.J., 2015. Persistence of dissolved organic matter in lakes related to its molecular characteristics. *Nature Geosci* **8**, 454–457. https://doi.org/10.1038/ngeo2440 http://www.nature.com/ngeo/journal/v8/n6/abs/ngeo2440.html#supplementary-information
Kew, W., Blackburn, J.W.T., Uhrin, D., 2018. Response to comment on "laser desorption/ionization coupled to FTICR mass spectrometry for studies of natural organic matter". *Anal Chem* **90**, 5968–5971.
Kim, S., Kramer, R.W., Hatcher, P.G., 2003. Graphical Method for Analysis of Ultrahigh-Resolution Broadband Mass Spectra of Natural Organic Matter, the Van Krevelen Diagram. *Anal Chem* **75**, 5336–5344. https://doi.org/10.1021/ac034415p
Klaas G. J. Nierop, *, Caroline M. Preston, ‡ and, Joeri Kaal†, §, 2005. Thermally Assisted Hydrolysis and Methylation of Purified Tannins from Plants. https://doi.org/10.1021/AC050564R
Kleber, M., 2010. What is recalcitrant soil organic matter? *Environmental Chemistry* **7**, 320–332.
Kleber, M., Lehmann, J., 2019. Humic Substances Extracted by Alkali Are Invalid Proxies for the Dynamics and Functions of Organic Matter in Terrestrial and Aquatic Ecosystems. *J Environ Qual* **48**, 207–216. https://doi.org/10.2134/jeq2019.01.0036
Koch, B.P., Dittmar, T., 2006. From mass to structure: an aromaticity index for high-resolution mass data of natural organic matter. *Rapid Communications in Mass Spectrometry* **20**, 926–932. https://doi.org/10.1002/rcm.2386

Koch, B.P., Dittmar, T., Witt, M., Kattner, G., 2007. Fundamentals of Molecular Formula Assignment to Ultrahigh Resolution Mass Data of Natural Organic Matter. *Anal Chem* **79**, 1758–1763. https://doi.org/10.1021/ac061949s

Kolattukudy, P.E., 2001. Polyesters in higher plants. In 'Biopolyesters'. Springer, pp. 1–49.

Kothawala, D.N., Kellerman, A.M., Catalán, N., Tranvik, L.J., 2020. Organic Matter Degradation across Ecosystem Boundaries: The Need for a Unified Conceptualization. *Trends Ecol Evol*.

Kuznetsova, O. V, Sevastyanov, V.S., Timerbaev, A.R., 2019. What are the current analytical approaches for sediment analysis related to the study of diagenesis? Highlights from 2010 to 2018. *Talanta* **191**, 435–442. https://doi.org/https://doi.org/10.1016/j.talanta.2018.08.080

LaRowe, D.E., Van Cappellen, P., 2011. Degradation of natural organic matter: a thermodynamic analysis. *Geochim Cosmochim Acta* **75**, 2030–2042.

Lee, Y., Lee, B., Hur, J., Min, J.O., Ha, S.Y., Ra, K., Kim, K.T., Shin, K.H., 2016. Biodegradability of algal-derived organic matter in a large artificial lake by using stable isotope tracers. *Environ Sci Pollut Res Int* **23**, 8358–8366. https://doi.org/10.1007/s11356-016-6046-1

Liu, S., Feng, W., Song, F., Li, T., Guo, W., Wang, B., Wang, H., Wu, F., 2019. Photodegradation of algae and macrophyte-derived dissolved organic matter: A multi-method assessment of DOM transformation. *Limnologica* **77**, 125683. https://doi.org/10.1016/J.LIMNO.2019.125683

Lützow, M. v, Kögel-Knabner, I., Ekschmitt, K., Matzner, E., Guggenberger, G., Marschner, B., Flessa, H., 2006. Stabilization of organic matter in temperate soils: mechanisms and their relevance under different soil conditions–a review. *Eur J Soil Sci* **57**, 426–445.

Martone, P.T., Estevez, J.M., Lu, F., Ruel, K., Denny, M.W., Somerville, C., Ralph, J., 2009. Discovery of Lignin in Seaweed Reveals Convergent Evolution of Cell-Wall Architecture. *Current Biology* **19**, 169–175. https://doi.org/10.1016/J.CUB.2008.12.031

McCallister, S.L., Ishikawa, N.F., Kothawala, D.N., 2018. Biogeochemical tools for characterizing organic carbon in inland aquatic ecosystems. *Limnol Oceanogr Lett* **3**, 444–457. https://doi.org/doi:10.1002/lol2.10097

van der Meij, W.M., Temme, A.J.A.M., Lin, H.S., Gerke, H.H., Sommer, M., 2018. On the role of hydrologic processes in soil and landscape evolution modeling: concepts, complications and partial solutions. *Earth Sci Rev*. https://doi.org/10.1016/j.earscirev.2018.09.001

Meyers, P.A., Ishiwatari, R., 1993. Lacustrine organic geochemistry—an overview of indicators of organic matter sources and diagenesis in lake sediments. *Org Geochem* **20**, 867–900. https://doi.org/http://dx.doi.org/10.1016/0146-6380(93)90100-P

Milliken, K.L., 2003. Late Diagenesis and Mass Transfer in Sandstone–Shale Sequences. *Treatise on Geochemistry* 159–190. https://doi.org/10.1016/B0-08-043751-6/07091-2

Mopper, K., Stubbins, A., Ritchie, J.D., Bialk, H.M., Hatcher, P.G., 2007. Advanced Instrumental Approaches for Characterization of Marine Dissolved Organic Matter: Extraction Techniques, Mass Spectrometry, and Nuclear Magnetic Resonance Spectroscopy. *Chem Rev* **107**, 419–442. https://doi.org/10.1021/cr050359b

Moran, M.A., Sheldon Jr., W.M., Zepp, R.G., 2000. Carbon loss and optical property changes during long-term photochemical and biological degradation of estuarine dissolved organic matter. *Limnol Oceanogr* **45**, 1254–1264. https://doi.org/doi:10.4319/lo.2000.45.6.1254

784 Moran, M.A., Zepp, R.G., 1997. Role of photoreactions in the formation of biologically labile
785 compounds from dissolved organic matter. *Limnol Oceanogr*.
786 https://doi.org/10.4319/lo.1997.42.6.1307
787 Mueller, K.E., Polissar, P.J., Oleksyn, J., Freeman, K.H., 2012. Differentiating temperate tree
788 species and their organs using lipid biomarkers in leaves, roots and soil. *Org Geochem*
789 **52**, 130–141.
790 Navel, S., Mermillod-Blondin, F., Montuelle, B., Chauvet, E., Marmonier, P., 2012.
791 Sedimentary context controls the influence of ecosystem engineering by bioturbators on
792 microbial processes in river sediments. *Oikos* **121**, 1134–1144.
793 https://doi.org/doi:10.1111/j.1600-0706.2011.19742.x
794 Nierop, K.G.J., Verstraten, J.M., 2004. Rapid molecular assessment of the bioturbation extent
795 in sandy soil horizons under pine using ester-bound lipids by on-line thermally assisted
796 hydrolysis and methylation-gas chromatography/mass spectrometry. *Rapid*
797 *Communications in Mass Spectrometry* **18**, 1081–1088.
798 https://doi.org/10.1002/rcm.1449
799 Patriarca, C., Balderrama, A., Može, M., Sjöberg, P.J.R., Bergquist, J., Tranvik, L.J.,
800 Hawkes, J.A., 2020. Investigating the ionization of dissolved organic matter by
801 electrospray ionization. *Anal Chem* acs.analchem.0c03438.
802 https://doi.org/10.1021/acs.analchem.0c03438
803 Repeta, D.J., 2015. Chapter 2 - Chemical Characterization and Cycling of Dissolved Organic
804 Matter A2 - Hansell, Dennis A. In 'Biogeochemistry of Marine Dissolved Organic
805 Matter (Second Edition)' (Ed. Carlson, C.A.). Academic Press, Boston, pp. 21–63.
806 https://doi.org/https://doi.org/10.1016/B978-0-12-405940-5.00002-9
807 Sankar, M.S., Dash, P., Singh, S., Lu, Y., Mercer, A.E., Chen, S., 2019. Effect of photo-
808 biodegradation and biodegradation on the biogeochemical cycling of dissolved organic
809 matter across diverse surface water bodies. *Journal of Environmental Sciences*.
810 https://doi.org/https://doi.org/10.1016/j.jes.2018.06.021
811 Solihat, N.N., Acter, T., Kim, D., Plante, A.F., Kim, S., 2019. Analyzing Solid-Phase Natural
812 Organic Matter Using Laser Desorption Ionization Ultrahigh Resolution Mass
813 Spectrometry. *Anal Chem* **91**, 951–957. https://doi.org/10.1021/acs.analchem.8b04032
814 Stubbins, A., Dittmar, T., 2014. Dissolved Organic Matter in Aquatic Systems.
815 https://doi.org/10.1016/B978-0-08-095975-7.01010-X
816 Vähätalo, A. V, Aarnos, H., Mäntyniemi, S., 2010. Biodegradability continuum and
817 biodegradation kinetics of natural organic matter described by the beta distribution.
818 *Biogeochemistry* **100**, 227–240.
819 Valle, J., Gonsior, M., Harir, M., Enrich-Prast, A., Schmitt-Kopplin, P., Bastviken, D.,
820 Conrad, R., Hertkorn, N., 2018. Extensive processing of sediment pore water dissolved
821 organic matter during anoxic incubation as observed by high-field mass spectrometry
822 (FTICR-MS). *Water Res* **129**, 252–263.
823 https://doi.org/https://doi.org/10.1016/j.watres.2017.11.015
824 Wakeham, S.G., Ertel, J.R., 1988. Diagenesis of organic matter in suspended particles and
825 sediments in the Cariaco Trench. *Org Geochem* **13**, 815–822.
826 Ward, N.D., Bianchi, T.S., Sawakuchi, H.O., Gagne-Maynard, W., Cunha, A.C., Brito, D.C.,
827 Neu, V., de Matos Valerio, A., da Silva, R., Krusche, A. V, 2016. The reactivity of
828 plant-derived organic matter and the potential importance of priming effects along the
829 lower Amazon River. *J Geophys Res Biogeosci* **121**, 1522–1539.
830 Ward, N.D., Morrison, E.S., Liu, Y., Rivas-Ubach, A., Osborne, T.Z., Ogram, A. V., Bianchi,
831 T.S., 2019. Marine microbial community responses related to wetland carbon

mobilization in the coastal zone. *Limnol Oceanogr Lett* **4**, 25–33. https://doi.org/10.1002/lol2.10101
Wershaw, R.L., 2004. Evaluation of conceptual models of natural organic matter (humus) from a consideration of the chemical and biochemical processes of humification.
Wetzel, R.G., 2001. Limnology: Lake and River Ecosystems, 3rd. *Acadimic pres, AQn Elsevier imprint, Sanfrancisco, New York, London*.
Willers, C., Jansen van Rensburg, P.J., Claassens, S., 2015. Phospholipid fatty acid profiling of microbial communities–a review of interpretations and recent applications. *J Appl Microbiol* **119**, 1207–1218.
Williams, J.S., Dungait, J.A.J., Bol, R., Abbott, G.D., 2016. Contrasting temperature responses of dissolved organic carbon and phenols leached from soils. *Plant Soil* **399**, 13–27.
Youngblood, W.W., Blumer, M., Guillard, R.L., Fiore, F., 1971. Saturated and unsaturated hydrocarbons in marine benthic algae. *Mar Biol* **8**, 190–201. https://doi.org/10.1007/BF00355215
Zhuang, W.-E., Chen, W., Cheng, Q., Yang, L., 2021. Assessing the priming effect of dissolved organic matter from typical sources using fluorescence EEMs-PARAFAC. *Chemosphere* **264**, 128600. https://doi.org/10.1016/j.chemosphere.2020.128600

Fig. 1 Distribution in compounds classes of all the artificial sediments for both oxygen conditions (i.e., oxic and anoxic). Characteristics of compound classes are presented in Table A.2.

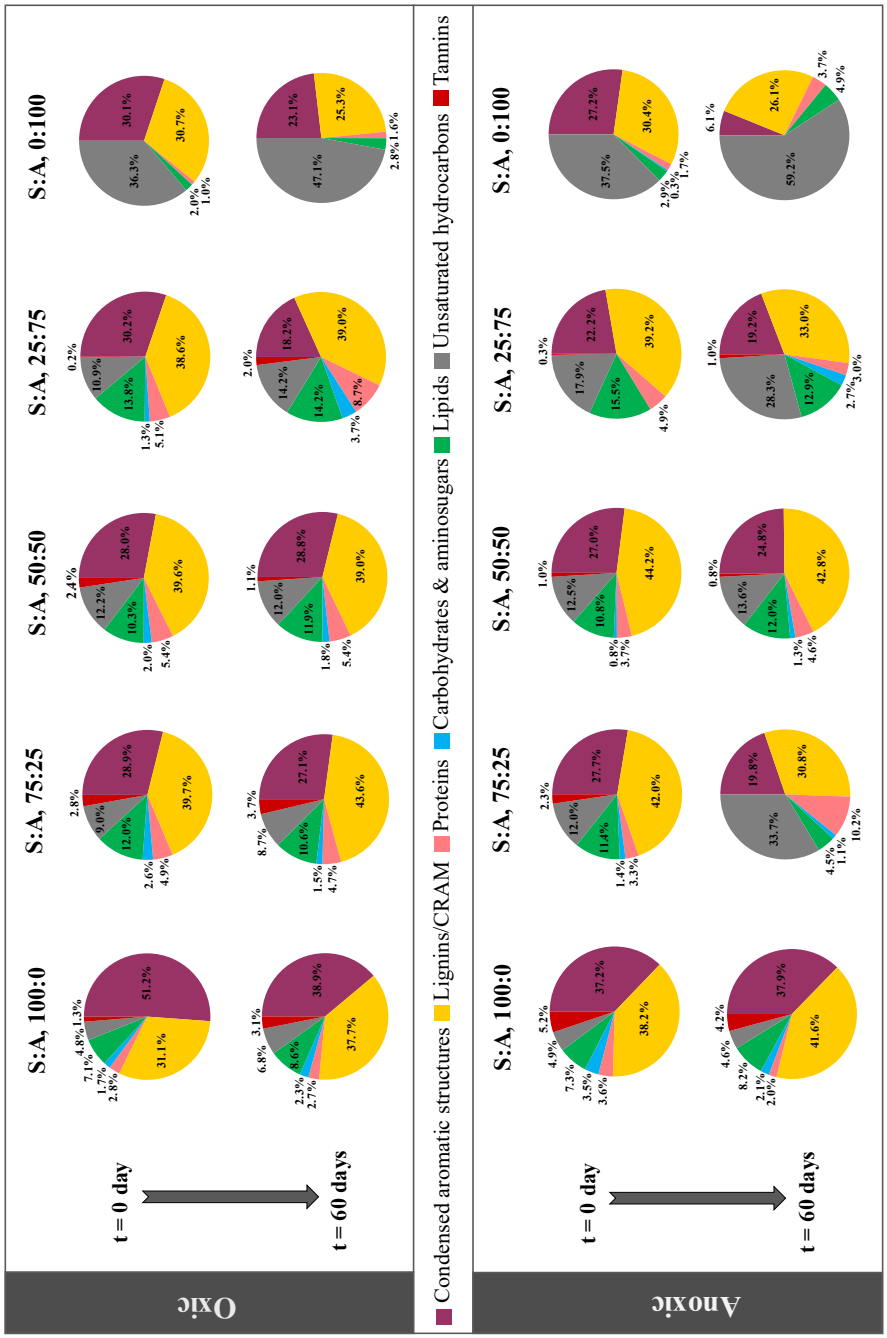

884 **Fig. 2** Relative proportions of the chemical families identified by the THM–GC–MS analysis of the
885 end members at t = 0 day and t = 60 days in all the artificial sediments for both oxygen conditions
886 (i.e., oxic and anoxic). Uncertainties are the standard deviation of two experimental replicates.
887 Asterisks was added on data where a significant difference (p-value < 0.05) is observed between day 0
888 and day 60.

889

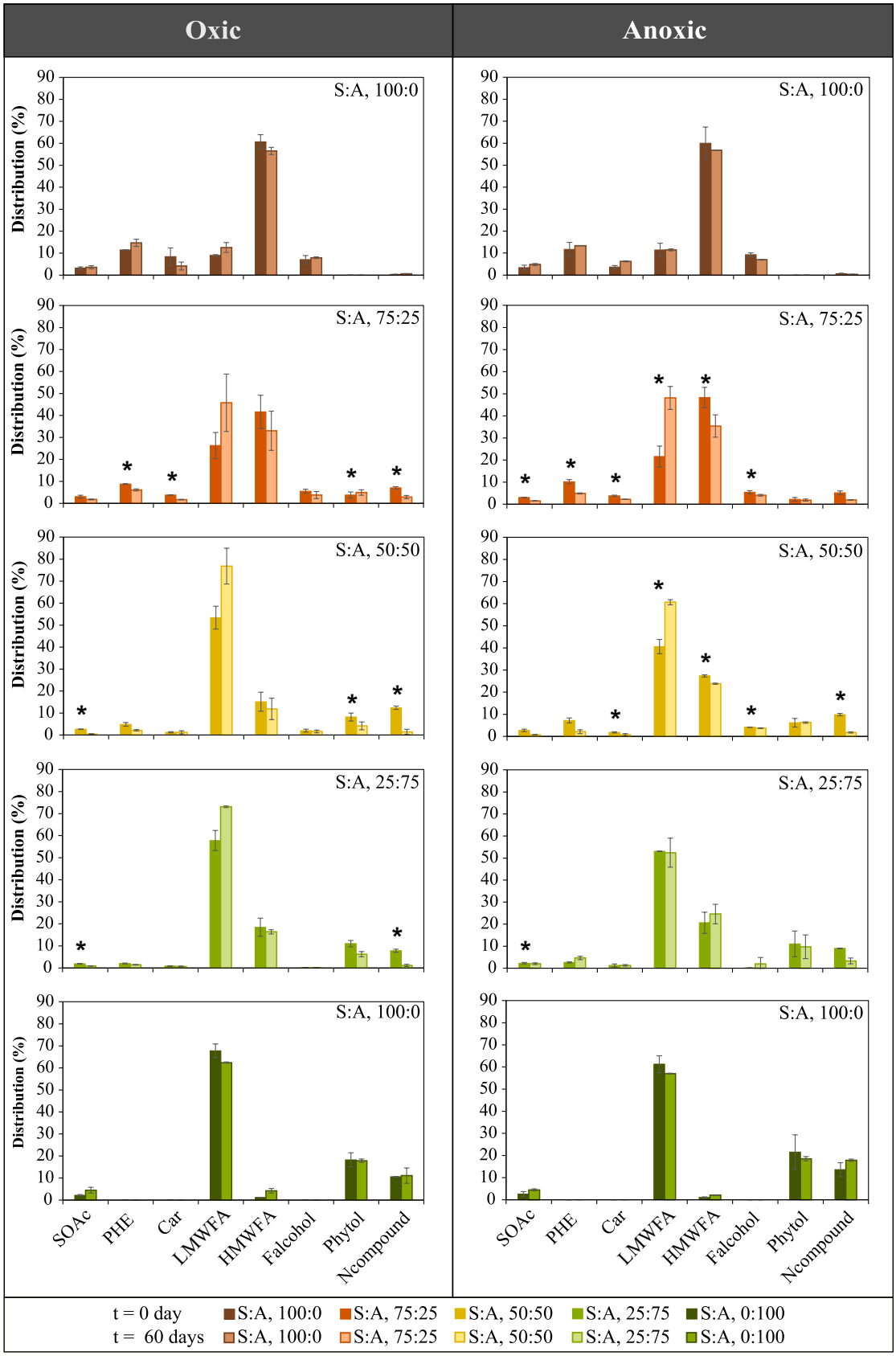
Oxic
Anoxic
Distribution (%)
S:A, 100:0
S:A, 75:25
S:A, 50:50
S:A, 25:75
S:A, 100:0
SOAc
PHE
Car
LMWFA
HMWFA
Falcohol
Phytol
Ncompound
t = 0 day
t = 60 days
S:A, 100:0
S:A, 75:25
S:A, 50:50
S:A, 25:75
S:A, 0:100

Fig. 3 Principal coordinate analysis ordination of the Bray-Curtis dissimilarity matrix computed for the LDI FT–ICR MS data.

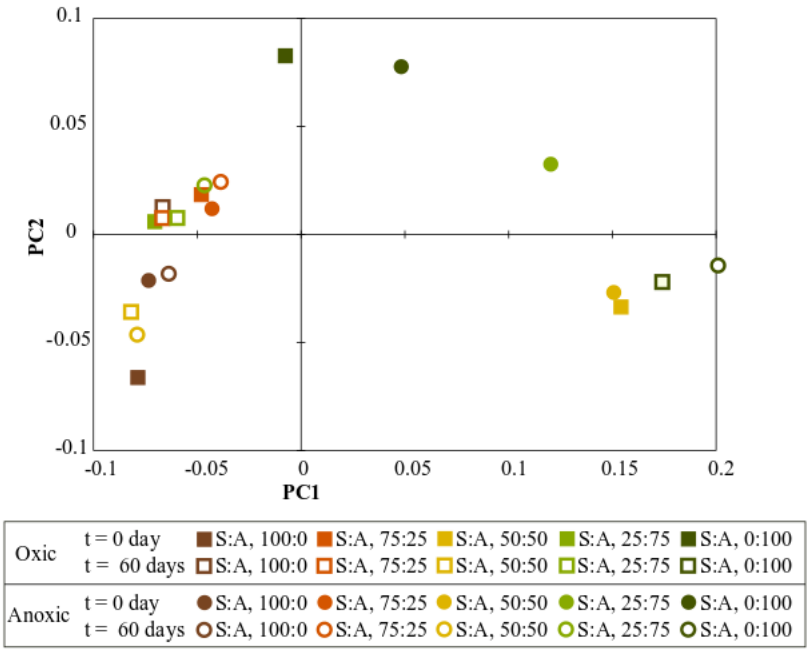

Fig. 4 Principal component analysis performed with the distribution of biomarker (67). Purple pentagons are the theoretical points of the S:A mixed samples calculated using an end-member mixing approach. Grey shapes highlight the groups identified by the hierarchical analysis classification.

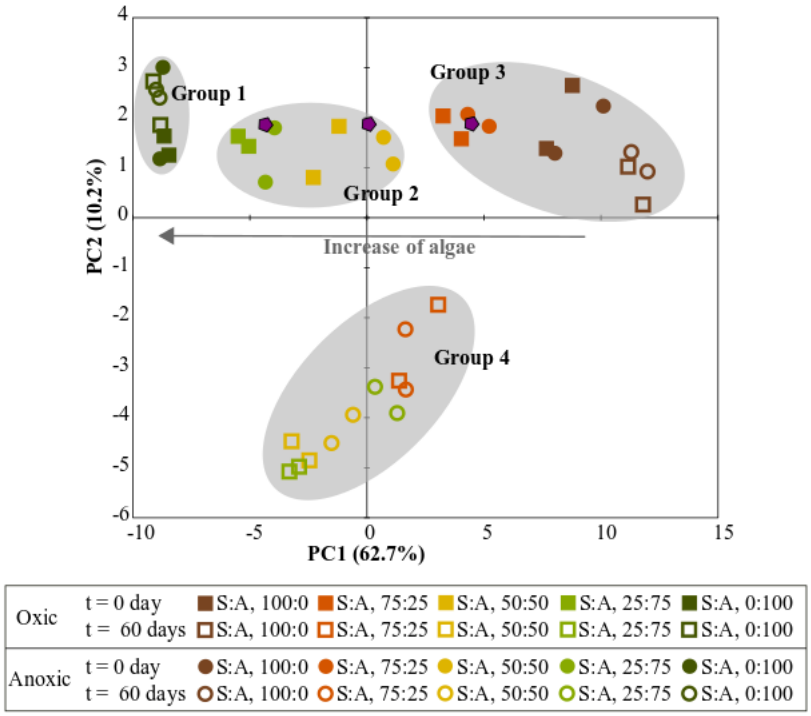

911 **Fig. 5** Principal component analysis performed with the distribution of microbial fatty acids
912 biomarker (11). Grey shapes highlight the groups identified by the hierarchical analysis classification.

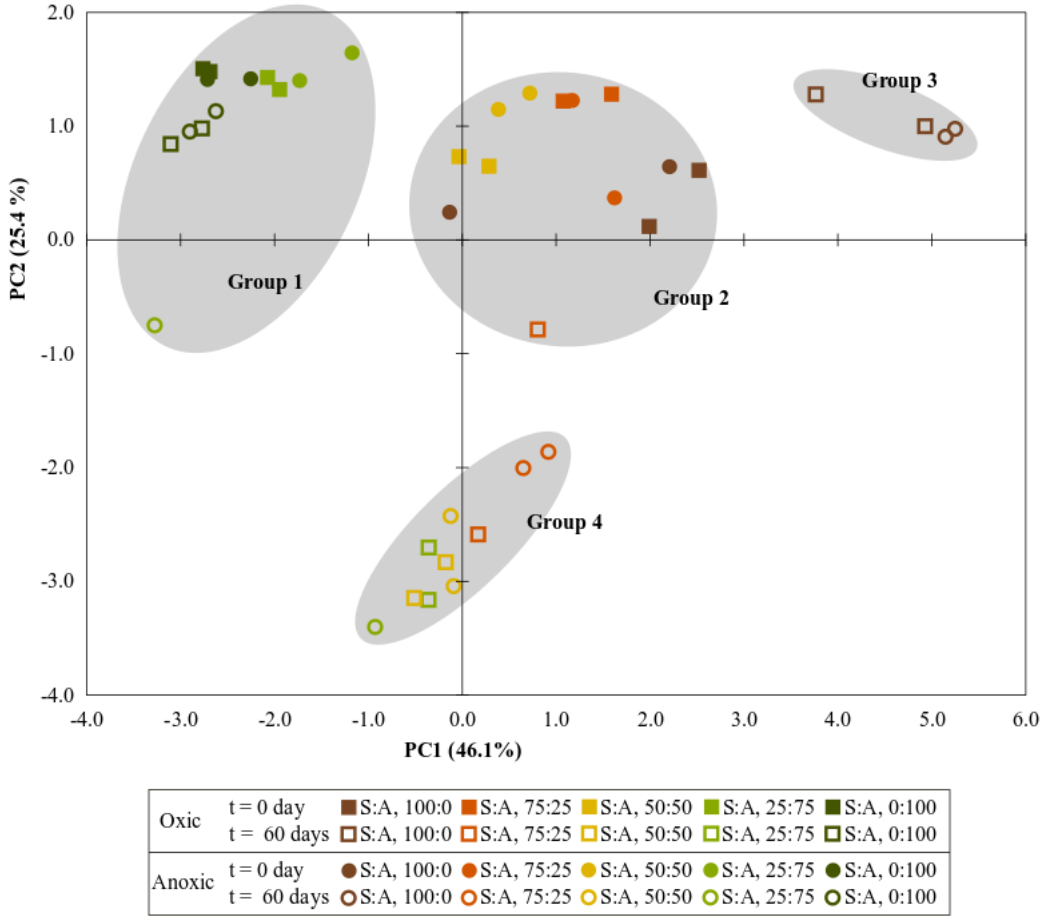

913